Supporting Information for: A Few Key Residues Determine the High Redox Potential Shift in Azurin Mutants

Laura Zanetti-Polzi,[*a] Carlo A. Bortolotti,[b] Isabella Daidone[c], Massimiliano Aschi[c], Andrea Amadei[d] and Stefano Corni[a]

1 The Quantum Centre

1.1 Choice of the QC

In Figure 1, the atoms included in the quantum centre for WT Az (panel A) and for the two mutants (panel B) are schematically shown. The choice of such a QC arises from tests on three different QCs.

As a general rule, in the framework of a typical QM/MM approach, the QC is chosen as the minimal part of the system necessary to properly describe the chemical reaction under investigation. In the case of the PMM-MD procedure an additional prerequisite is also requested: the size of the QC should allow the computational evaluation of a reasonably large set of unperturbed Hamiltonian eigenstates (13 in the present case) with a reasonably-sized atomic basis set at an affordable computational cost. In present case, a first QC (QC1) was tested including only the copper and its five ligands. The tests performed on QC1 provided an underestimation of the reduction potential of ≈ 0.45 V. A bigger QC (QC2) was thus tested including also the alpha carbon and the backbone nitrogen of residue 47, as the backbone nitrogen of residue 47 is at a distance of ≈ 3.6 nm from the sulphur of the ligand Cys 112. The inclusion of this portion of residue 47 improves the agreement with the experimental data leading to a smaller underestimation of the absolute value of the reduction potential (≈ 0.25 V as reported in the main manuscript). Such a choice is also in line with experimental indications on the importance of the hydrogen bonding pattern of residue 47 in lending rigidity to the active site.[1]

The backbone nitrogen of residue 114 is at a similar distance (≈ 3.5 nm) from the sulphur of Cys 112. Some tests were thus performed including also the alpha carbon and the backbone nitrogen of residue 114 in the QC (QC3). The tests on QC3 provided a reduction potential underestimated by ≈ 0.15 V, thus slightly improving the agreement with the experimental data. However, the interaction between the backbone nitrogen of residue 114 and the sulphur of Cys 112 is known to be unstable upon some mutations of residue 114 (*i.e*, the F114P mutation[1,2]). Considering that the main focus of the present analysis are the reduction potential shifts upon mutation, that are very well reproduced with QC2, and not the absolute values of the reduction potentials, the computationally more affordable QC2 was chosen for all the subsequent calculations and analyses. Such a choice allows indeed the prospective use of the same QC for different mutations taking into account the effect of the broken 112-114 interaction on the electronic states of the QC , warranting homogeneous results.

1.2 Quantum Centre parameters

As mentioned in the main text, for the MD simulations the bond lengths and bond angles between the copper and its ligands are set at the crystallographic values using the structures available for Wt Az and Mut1 (4AZU and 3JT2, respectively). As for Mut2 no crystallographic structure was available and as Mut1 and Mut2 share the same active site, the same parameters were used for the two mutants. In Tables 1 and 2 the bond lengths and bond angles of the crystallographic structures used for WT Az and the two mutants, respectively, are reported and compared to the ones obtained with the

[a]Center S3, CNR-Institute of Nanoscience , Via Campi 213/A, 41125, Modena, Italy.

[*]E-mail: laura.zanettipolzi@nano.cnr.it

[b]Department of Life Sciences, University of Modena and Reggio Emilia, Via Campi 183, 41125, Modena, Italy.

[c]Department of Physical and Chemical Sciences, University of L'Aquila, via Vetoio (Coppito 1), 67010, L'Aquila, Italy

[d]Department of chemical and Technological Sciences, University of Rome "Tor Vergata", Via della Ricerca Scientifica, 00185, Rome, Italy.
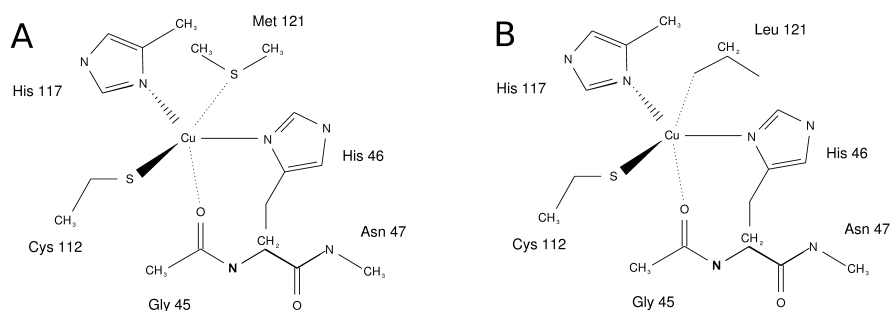
**Fig. 1** QC for WT Az (panel A) and Mut1-Mut2 (panel B).

QM/MM geometry optimisation of the quantum centres and to the average ones of the MD simulations. In Figures 2 and 3 a graphical comparison of the same structures is also provided.

Table 1 Comparison between the bond lengths and bond angles of the crystallographic structure of WT Az (4AZU), the values obtained by the QM/MM geometry optimisation in the oxidised (Ox.) and reduced (Red.) states of the QC and the average values of the MD simulations of WT Az in the reduced and oxidised ensemble. As specified in the main text, the bond lengths for the copper ligands are fixed in the MD simulations at the crystallographic value
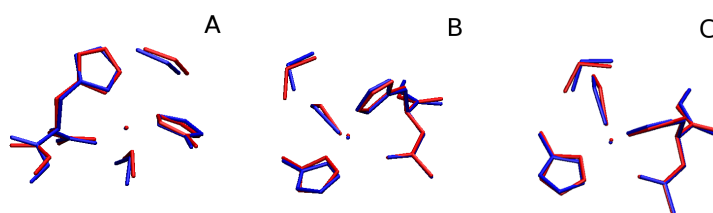
	crystallographic structure	QM/MM optimised geometry		MD simulations	
		Ox. active site	Red. active site	Ox. ensemble	Red. ensemble
Bonds(Å)					
$45O$-Cu	2.84	2.52	2.62		
$46N_\delta$-Cu	1.99	2.01	2.08		
$112S_\gamma$-Cu	2.27	2.23	2.34		
$117N_\delta$-Cu	2.11	1.98	2.02		
$121S_\delta$-Cu	3.18	3.26	3.19		
Angles (degrees)					
$O45$-Cu-$46N_\delta$	76	77	79	72	70
$O45$-Cu-$117N_\delta$	90	86	85	87	87
$O45$-Cu-$112S_\gamma$	99	102	97	114	114
$C45$-$O45$-Cu	134	136	135	136	136
$46N_\delta$-Cu-$117N_\delta$	104	107	109	102	100
$46N_\delta$-Cu-$112S_\gamma$	132	124	125	132	134
$46N_\delta$-Cu-$121S_\delta$	75	74	73	70	72
$46C_\varepsilon$-$46N_\delta$-Cu	123	123	126	122	122
$46C_\gamma$-$46N_\delta$-Cu	132	129	126	130	130
$112S_\gamma$-Cu-$117N_\delta$	124	128	125	124	124
$112S_\gamma$-Cu-$121S_\delta$	110	104	109	100	99
$112C_\beta$-$112S_\gamma$-Cu	109	114	110	114	113
$117N_\delta$-Cu-$121S_\delta$	84	93	92	89	90
$117C_\varepsilon$-$117N_\delta$-Cu	125	125	125	122	122
$117C_\gamma$-$117N_\delta$-Cu	129	126	127	129	129
$121C_\gamma$-$121S_\delta$-Cu	138	144	138	137	138
$121C_\varepsilon$-$121S_\delta$-Cu	99	100	100	93	94

Table 2 Comparison between the bond lengths and bond angles of the crystallographic structure of Mut1 (3JT2), the values obtained by the QM/MM geometry optimisation in the oxidised (Ox.) and reduced (Red.) states of the QC and the average values of the MD simulations of Mut1 and Mut2 in the reduced and oxidised ensemble. As specified in the main text, the bond lengths for the copper ligands are fixed in the MD simulations at the crystallographic value

	crystallographic structure	QM/MM optimised geometry		Mut1 MD simulations		Mut2 MD simulations	
		Ox. active site	Red. active site	Ox. ensemble	Red. ensemble	Ox. ensemble	Red. ensemble
Bonds (Å)							
45O-Cu	2.30	2.25	2.36				
46N$_\delta$-Cu	1.97	2.01	2.05				
112S$_\gamma$-Cu	1.99	2.21	2.31				
117N$_\delta$-Cu	1.96	1.97	2.01				
121C$_\delta$-Cu	4.16	4.12	3.93				
Angles (degrees)							
O45-Cu-46N$_\delta$	80	90	91	79	77	78	78
O45-Cu-117N$_\delta$	101	99	96	99	102	101	103
O45-Cu-112S$_\gamma$	105	93	89	108	108	110	110
C45-O45-Cu	143	135	131	146	147	146	147
46N$_\delta$-Cu-117N$_\delta$	108	106	109	111	112	112	114
46N$_\delta$-Cu-112S$_\gamma$	129	126	128	126	125	125	123
46N$_\delta$-Cu-121C$_\delta$	81	71	74	78	76	103	85
46C$_\epsilon$-46N$_\delta$-Cu	111	119	119	114	114	114	113
46C$_\gamma$-46N$_\delta$-Cu	142	132	131	139	138	139	139
112S$_\gamma$-Cu-117N$_\delta$	120	126	123	119	119	117	118
112S$_\gamma$-Cu-121C$_\delta$	105	109	113	101	104	102	107
112C$_\beta$-112S$_\gamma$-Cu	119	113	107	122	121	121	121
117N$_\delta$-Cu-121C$_\delta$	63	74	74	72	70	73	79
117C$_\epsilon$-117N$_\delta$-Cu	119	127	126	123	124	121	122
117C$_\gamma$-117N$_\delta$-Cu	128	124	125	128	127	129	129
121C$_\gamma$-121C$_\delta$-Cu	107	113	116	111	113	110	114
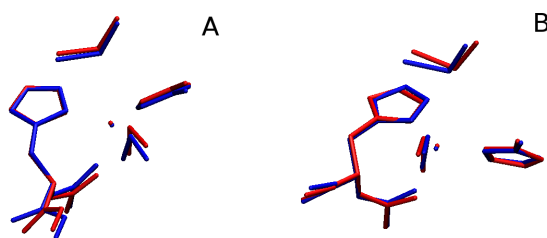
Fig. 2 Comparison between the crystallographic structure of the active site of WT Az (in red), the structure obtained from the ONIOM optimisation in the oxidised state (in blue, panel A) and the average structure in the MD simulation of WT Az in the oxidised ensemble (in blue, panel B). The deviations in the reduced state of the active site are comparable to the ones shown here.


Fig. 3 Comparison between the crystallographic structure of the active site of Mut1 (in red), the structure obtained from the ONIOM optimisation in the oxidised state (in blue, panel A) and the average structures in the MD simulation of Mut1 (in blue, panel B) and Mut2 (in blue, panel C) in the oxidised ensemble. The deviations in the reduced state of the active site are comparable to the ones shown here.

1.3 Interaction between the copper and the axial ligand Leu121

In both Mut1 (N47S/M121L) and Mut2 (N47S/F114N/M121L) the weak axial ligand Met121 is replaced by a Leu. The interaction between Leu and the copper is even weaker and thus the choice of constraining the bond length at the crystallographic value for the mutated residue, as done for Met121, is not straightforward. To evaluate the appropriateness of binding the Leu side chain to the copper, the energy difference between the crystallographic active site and an active site structure in which Leu is not interacting with the copper is calculated. To break the interaction between the axial ligand and the copper, the torsional dehydrate that determines the orientation between the side chain and the backbone is rotated enlarging the distance between the aliphatic groups and the copper (see Figure 4). Such a structure is then refined by performing quantum-chemical geometry optimisation with the ONIOM computational technique (see main text). The active site ground state energy is then evaluated in vacuum with the M06 functional and a TZV basis set and compared to the corresponding one obtained with the crystallographic structure. Such a calculation shows that the crystallographic geometry has a ≈70 kJ/mol lower energy than the rotated one. While the exact nature of the interaction between the Leu side chain and Cu is unclear, this energy difference is consistent with the presence of an agostic interaction between the metal and the aliphatic side chain.[3] On the basis of this calculation a bond is added between the copper and Leu at the crystallographic bond length.

2 Effect of the N47S Mutation in the N47S/F114N/M121L Mutant

The analysis performed for Mut1 to understand the effect of the N47S mutation on the interaction between the two loops containing the ligands (see main text) is repeated for Mut2 providing the same results. In Figure 5 the distribution of the distances sampled along the trajectory between the side-chain oxygen of residue 47 and both the sulphur of Cys112 (OS distance) and the backbone nitrogen of Thr113 (ON distance) are reported for Mut2 in the reduced (panel A) and in the oxidised (panel B) ensemble in the two ionic atmospheres. The results are analogous to the ones obtained for Mut1.
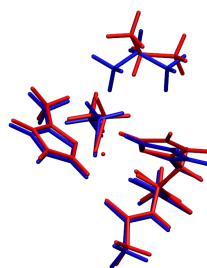
Fig. 4 Schematic representation of the crystallographic active site (blue) and of the active site with the rotated Leu side chain (red) after the ONIOM geometry optimisation.
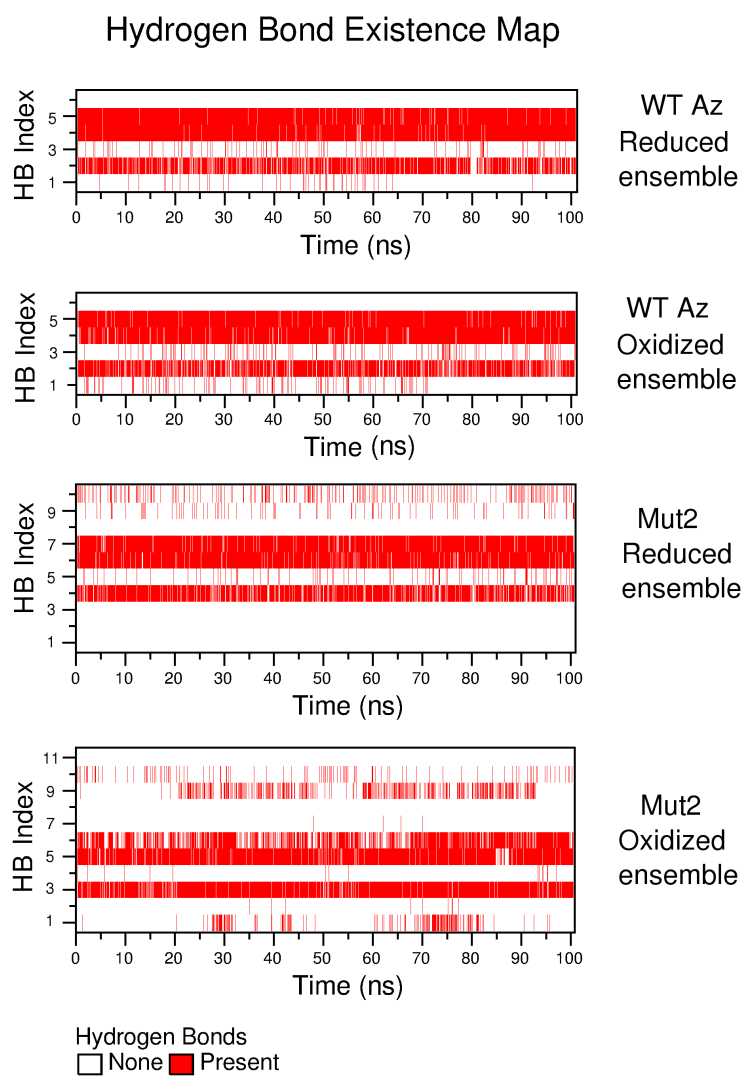
As for Mut1, E^0 is calculated on two subpopulations: the first at small ON/OS distances and the second at large OS/ON distances (see main text). Similarly to what observed for Mut1, higher ON/OS distances correspond to a 165 mV higher E^0. It has to be pointed out that such a calculation is less insightful for Mut2 as effects on $\Delta\varepsilon$ due to the F114N mutation (uncorrelated with the ON/OS distances) are obviously expected.
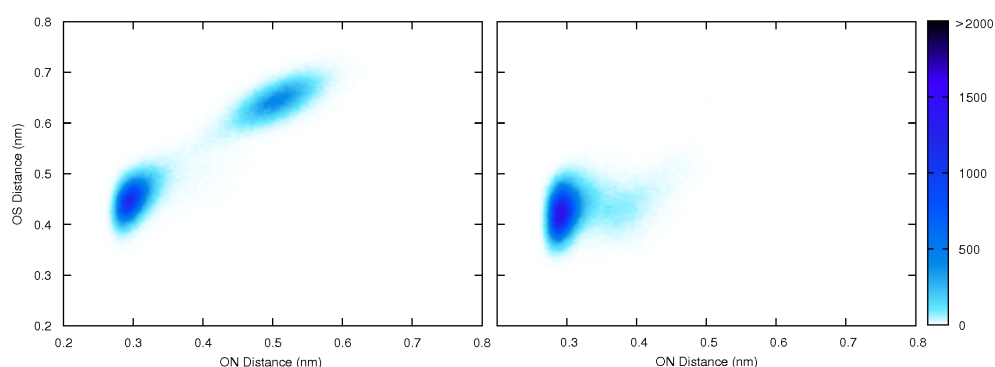
Fig. 5 Colour maps representing the distribution of distances between loop 1 and loop 2 along the MD simulations of Mut2 in the reduced (panel A) and oxidised (panel B) ensembles. "ON Distance" refers to the distance between the side-chain oxygen of residue 47 and the backbone nitrogen of Thr 113; "OS Distance" refers instead to the distance between the same oxygen and the sulphur of Cys112.Three dimensional plot of the distances sampled along the trajectories between residue 47 and both Cys112 and Thr113. The colour code represents the number of points at the corresponding ON/OS distances.

3   Hydrogen bonding pattern of His117

In order to check whether the F114N mutation affects the hydrogen bonding (HB) pattern of the planar strong copper ligand His117 the GROMACS tools are applied to the trajectories of WT Az and Mut1 (in the oxidised and reduced ensembles and in the two ionic states) to obtain the HB map of the residue during the MD simulation. The results, reported in Figure 6, show that the mutation does not affect such a HB pattern. In both variants His117 shows indeed the same three stable HBs: between the backbone nitrogen of His117 and the backbone oxygen of residue 114, between the backbone oxygen of His112 and the backbone nitrogen of both residue 120 and 121. Note that in the Figure the HB maps for the simulations performed in the ionic ensemble that neutralises the oxidised state are reported. The analysis was performed also for the simulations in the other ionic state providing qualitatively equivalent results.

Hydrogen Bond Existence Map

WT Az Reduced ensemble

WT Az Oxidized ensemble

Mut2 Reduced ensemble

Mut2 Oxidized ensemble

Hydrogen Bonds
None   Present

Fig. 6 Hydrogen bond existence map for WT Az and Mut2 in the reduced and oxidised ensemble.

References

1 N. M. Marshall, D. K. Garner, T. D. Wilson, Y.-G. Gao, H. Robinson, M. J. Nilges and Y. Lu, *Nature*, 2009, **462**, 113–116.

2 C. Li, S. Yanagisawa, B. M. Martins, A. Messerschmidt, M. J. Banfield and C. Dennison, *Proc. Natl. Acad. Sci. USA*, 2006, **103**, 7258–7263.

3 G. R. Desiraju and T. Steiner, *Weak hydrogen bond*, Oxford University Press New York, 2001.